Metabolic Flux Analysis of Shewanella spp. Reveals Evolutionary Robustness in Central Carbon Metabolism

Yinjie J. Tang,[1,2] Hector Garcia Martin,[3,4] Paramvir S. Dehal,[1,3] Adam Deutschbauer,[1,3] Xavier Llora,[5] Adam Meadows,[6] Adam Arkin,[1,3,4,7] Jay. D. Keasling[1,3,4,7,8]

[1]Virtual Institute of Microbial Stress and Survival, Lawrence Berkeley National Laboratory, Berkeley, California 94720; telephone: 510-642-4862;

fax: 510-495-2630; e-mail: keasling@berkeley.edu

[2]Energy, Enviornmental and Chemical Engineering Department, Washington University, St. Louis, Missouri

[3]Physical Biosciences Division, Lawrence Berkeley National Laboratory, Berkeley, California 94720

[4]Joint BioEnergy Institute, 5885 Hollis, Emeryville, California 94608

[5]National Center for Supercomputing Applications, University of Illinois at Urbana-Champaign, Urbana, Illinois [6]Amyris Biotechnologies, Inc., Emeryville, California

[7]Department of Bioengineering, University of California, Berkeley, California

[8]Department of Chemical Engineering, University of California, Berkeley, California 94270

ABSTRACT: Shewanella spp. are a group of facultative anaerobic bacteria widely distributed in marine and fresh-water environments. In this study, we profiled the central metabolic fluxes of eight recently sequenced Shewanella species grown under the same condition in minimal med-ium with [3-^{13}C] lactate. Although the tested Shewanella species had slightly different growth rates (0.23–0.29 h^{-1}) and produced different amounts of acetate and pyruvate during early exponential growth (pseudo-steady state), the relative intracellular metabolic flux distributions were remarkably similar. This result indicates that Shewanella species share similar regulation in regard to central carbon metabolic fluxes under steady growth conditions: the maintenance of metabolic robustness is not only evident in a single species under genetic perturbations (Fischer and Sauer, 2005; Nat Genet 37(6):636–640), but also observed through evolutionary related microbial species. This remarkable conservation of relative flux profiles through phylogenetic differences prompts us to introduce the concept of metabotype as an alternative scheme to classify microbial fluxomics. On the other hand, Shewanella spp. display flexibility in the relative flux profiles when switching their metabolism from consuming lactate to consuming pyruvate and acetate.

Introduction

Shewanella spp. have received significant attention because of their versatile respiration and potential to engage in co-metabolic bioremediation of toxic metals, radionuclides, and halogenated organic compounds (Tiedje, 2002; Venka-teswaran et al., 1999). Shewanella can also be used in microbial fuel cell applications: via an electrode as a final electron acceptor, electricity can be harvested from biomass when they oxidize organic compounds (Fredrickson et al., 2008). In order to understand Shewanella metabolism and fully explore their bioremediation and bioenergy applica-tions, we first reported the metabolic fluxes in the model species S. oneidensis MR-1 under different growth condi-tions (Tang et al., 2007a). Metabolite fluxes represent the integrated functional output of the underlying metabolic network (Sauer, 2006) since they link genes, proteins, and metabolites to macroscopic biological functions. In this article, we further investigated the variation of central metabolic flux distribution in phylogenetically different Shewanella species to reveal the robustness of metabolic regulation, a long-recognized important property of biological systems. Previous studies using other micro-organisms have examined metabolic robustness to

pertur-bations in the form of mutations and environmental conditions (Blank et al., 2005; Fischer and Sauer, 2005). A relatively unstudied type of robustness, however, involves the change of metabolic fluxes across a clade of related species under similar environmental conditions. Recent sequencing of several of these Shewanella species gives us the opportunity to use the well-characterized Shewanella oneidensis MR1 as a basis to study the variation of central metabolic flux profiles across wide phylogenetic differences (Table I) (Fredrickson et al., 2008). The results may advance our understanding of the metabolic flux regulation in all Shewanella species and provide guidelines for rational genetic engineering of Shewanella species to improve their potential application in bioremediation and fuel cells.

Materials and Methods

Culture Conditions and Analytical Methods for Metabolites

The eight Shewanella species in this study (MR1, MR4, MR7, SB, CN, W3, ANA, PV4) were donated by the Shewanella Federation. E. coli K12 W3110 was obtained from The American Type Culture Collection (ATCC 27325). All species were cultured in the modified MR-1 defined medium (Tang et al. 2006) in shaking glass tubes (12 mL, duplicates) at 308C. The carbon source was [3-^{13}C] sodium L-lactate (98%, Cambridge Isotope, Andover, MA). The inoculum was prepared in LB medium overnight (optical density at a wavelength of 600 nm, OD_{600} > 1.5); the cultures were started with a 0.09% inoculation volume to minimize the inoculation effect. Total biomass growth in the minimal medium was monitored by measuring the OD_{600}, based on the correlation between dried biomass and its corresponding OD_{600}. The concentrations of lactate, acetate, and pyruvate in the medium were measured using enzyme kits (r-Biopharm, Darmstadt, Germany). The GC-MS protocol for isotopomer measurement has been described previously (Tang et al., 2007c). In brief, a 10-mL culture at the early exponential phase (OD_{600} ¼ 0.3–0.5) was harvested and hydrolyzed. GC-MS samples were prepared in tetrahydrofuran (THF) and N-(tert-butyldimethylsilyl)- N-methyl-trifluoroacetamide (Sigma-Aldrich, St. Louis, MO). GC-MS was carried out using a gas chromatograph (HP6890 series, Agilent, Inc., Santa Clara, CA) equipped with a DB5 column (J&W Scientific, Inc., Folsom, CA) and a mass spectrometer (5973 Network, Agilent, Inc.). Two types of positively charged species from the mass spectrometer were used for flux analysis: unfragmented molecules [-57] and fragmented species that had lost one carboxyl group [-159]. Corrections due to the natural abundance of isotopes were applied using the publicly available tool for mass isotopomer data (Wahl et al., 2004).

Algorithm for Flux Calculation and Isotopomer Modeling

Biochemical pathways for the central carbon metabolism of Shewanella and E. coli were obtained from the genome database MicrobesOnline (Alm et al., 2005) (Fig. 1). The metabolic network includes the tricarboxylic acid (TCA) cycle (including the glyoxylate shunt), C_1 metabolism, the Entner-Doudoroff (ED) pathway, gluconeogenesis, and the pentose phosphate (PP) pathway. Only a few reactions (the couples: 16–20, 15–19, 13–17, and 14–18, Fig. 1) were considered as reversible due to their significant impact on the isotopomer distribution. Reversible reactions in the pentose-phosphate pathway were not included, since the total flux through the PP pathway in this study was very low (<5% of total carbon flow) and mainly for biomass production (Arauzo-Bravo and Shimizu, 2003; Zhao and Shimizu, 2003). The lactate uptake and outgoing metabolite fluxes (i.e.,

pyruvate and acetate) were measured directly via enzyme assays. The final values for these external fluxes were chosen by optimizing the error function (see below) within their measurement errors (see Table S-I). Similarly, the fluxes to biomass pools were not fixed by measurement values, but were loosely constrained by the MR-1 or Escherichia coli biomass compositions (Table S-I), which were optimized by the model using isotopomer information (Tang et al., 2007a). The upper and lower limits for each intracellular and extracellular flux are shown in Supplementary Table S-I (i.e., the optimal fluxes were forced to be within the range of their upper and lower limits). Metabolic fluxes for all reactions in Figure 1 were calculated by

minimizing the error (or objective) function:

$$\text{"}\eth v\text{Þ} = \frac{\sum_{i}^{m} w_i \text{"}_i \eth v}{m} \quad (1)$$

$$\text{"} \quad v \quad v_{kj} \qquad M_{ij} \; \text{з} \; N_{ij}\eth v\text{Þ} \; 2 \quad (2)$$

$$1 \quad u \quad t \text{¼}$$

where the vector v were the unknown fluxes, M_{ij} were the measured GC-MS data for the fraction of molecules with j labeled carbons for the ith amino acid or fragmented amino acid, N_{ij} were the corresponding model-simulated MS data, d_{ij} were the corresponding data measurement errors, and m was the total number of MS measurements. Different weights w_i were used for each amino acid depending on its relative importance for the fit. For example, histidine was given a weight of 0.0025 because: (1) flux through pentose phosphate pathway (constrained by histidine) was minimal (mainly for biosynthesis) comparing to TCA cycle related pathways (constrained by other amino acids); (2) GC-MS signals for histidine were usually very weak and had high background noise (Antoniewicz et al., 2007); and (3) the histidine pathway is complicated since its biosynth-esis route is via both C1 metabolism and C5 metabolism, so a good fit for histidine is difficult. This is why it was given a lower weight in the fitting. The reactions serine ! glycine ! 5, 10-methyl-THF(C1 pool) were found to be highly reversible and the reversibility was growth rate dependent (Perrenoud and Sauer, 2005); thus, serine and glycine were given a weight of 0.25 because exchange dynamics not captured in the isotopomer measurement might be expected to distort the calculated flux values. The rest of the amino acids (glutamate, aspartate, alanine, and phenyalanine) were given a weight of 1 since those amino acids clearly reflected their precursors' labeling and had the isotopic steady state during the early growth period. The model did not include cofactor balances.

The carbon labeling expected from a flux profile v was calculated via the cumomer method (Wiechert et al., 1999). The vector v_{ind} was formed by the 16 independent fluxes, obtained automatically from the reaction network (Supplementary data Table II) through Gaus-sian elimination, plus the unlabeled fractions of CO_2 and C1, for a total of 18 independent variables. For each species, the minimization of the error function was performed through genetic algorithms (GA) (Goldberg, 1989). Variables being optimized were encoded using floating point numbers with the additional constraint that their values should belong to the [0,1] interval. The adapted operators used were tournament selection without replacement (s ¼ 4) (Goldberg, 1989; Sastry and Goldberg, 2001), simulated binary crossover (SBX) (Deb and Agarwal, 1995; Deb and Kumar, 1995) with

h_c ¼ 10, probability p_c ¼ 0.9, a polynomial crossover mutation (Deb, 2001) with h ¼ 20, and mutation probability P ¼ 0.1. The GA was run for 325 iterations.

In tournament selection without replacement and with tournament size s, s chromosomes (solutions to the optimization problem) are chosen at random without replacement and entered into a tournament against each other. The best (low error) individual in the group of chromosomes wins the tournament and is selected into a mating pool for evolving new solutions. In SBX, individuals in the mating pool are divided into random pairs and each pair undergoes recombination with a probability p_c. For each pair participating in the crossover, each gene (or variable) undergoes a contracting or expanding crossover operation with a probability 0.5. Therefore, for each pair of chromosomes undergoing recombination, on average half of the genes are modified using either contracting or expanding crossover operations. The operations are designed to mimic crossover operator behavior on binary domains. The polynomial mutation is similar to SBX, and the only difference is in the computation of the polynomial probability. Instead of using genotypic distance between two parents as in SBX, the distance between a gene and its corresponding upper or lower bound, whichever is closer, is considered in computing the contracting and expanding probability distributions. In polynomial mutation, each gene (or variable) undergoes contracting or expanding operation with a probability p. The simulations were run until the error function did not decrease further with additional time steps and convergence was apparent. Supplementary files (Figs. S-1 and S-2) showed the optimized flux results and final fits of isotopomer data for each strain in our flux distribution calculation.

A Monte Carlo method was used to determine the confidence interval of all calculated fluxes (Zhao and Shimizu, 2003). The reliability of the results was gauged by changing the GC-MS data randomly within the measure-ment errors and running simulated annealing processes starting in the vicinity of the previously calculated optimum solution (Press et al., 1992) until the error function did not decrease any further and the processes converged (data not shown). The simulated annealing algorithm was used in statistic analysis of model results because this method was faster than genetic algorithm although less efficient in exploring the full flux space (hence the start point near the previously calculated optimum solution). Each of the individual simulated annealing processes performed 10,000 error function evaluations with an initial tempera-
ture of T_{ini} ¼ 3.0 and a final one of T_{fin} ¼ 0.05 (the scheme that showed the best results) and K ¼ 100 cooling steps
following an exponentially decreasing process for T_i. The initial independent flux vector v_{ind} was chosen to be that of the solution v for each species found through genetic algorithms with a random noise of maximum value d ¼ 0.05 added to each flux component so that the final solution was not trivially close to the original solution. This procedure was repeated 100 times, and the standard deviation for fluxes obtained (v_i) was determined as usual:

$$v_i = \sqrt{\frac{\sum_{t=1}^{100} (v_i - \bar{v})^2}{100}} \quad (3)$$

Results and Discussion

Although we tested 11 sequenced Shewanella spp., only eight of them were able to grow aerobically in a minimal lactate medium under 308C (the 11 Shewanella spp. listed in Fig. 2). The flux analysis experiments involved eight Shewanella spp. and E. coli W3110 grown in minimal medium containing 30 mM [3-^{13}C] lactate (Table I and Fig. 3a). The doubling times during the early exponential growth phases for all Shewanella spp. ranged from 2.3 to 2.9 h (3.2 h for E. coli as a comparison). In early exponential phase, Shewanella produced a significant amount of pyruvate and acetate, while E. coli excreted only acetate (Fig. 3b). Shewanella spp. grew faster in early log phase (OD_{600} < 0.5) than during the late log phase when it transitioned from growth on lactate to the less energetically favorable carbon sources pyruvate and acetate.

We calculated the flux distributions for all Shewanella spp. and E. coli (lactate uptake flux, v_1, was normalized to 1) and confidence intervals were calculated as described in Materials and Methods Section (Table II). The fits of the isotopomer data for flux calculations in all strains (supplementary Fig. S-2) showed a good agreement between predicted and measured isotopomer data with the exception of histidine (given a lower weight in the fitting), the labeling of which could not be predicted accurately due to isotopomer measurement uncertainty and the confounding effects of C1 metabolism for histidine synthesis not taken into account in the model.

In the early exponential phases, all Shewanella spp. showed similar intracellular flux profiles. The TCA cycle was not the main carbon metabolism route (fluxes <40% of lactate uptake), as much of the lactate was excreted as acetate (30–50% of lactate uptake) and pyruvate (10–20% of lactate uptake). S. oneidensis MR4 and S. oneidensis MR7 produced the most acetate and pyruvate, consistent with their highest growth rates among all tested Shewanella species. In contrast, E. coli W3110 excreted a large amount of acetate (47% of lactate uptake) and no pyruvate in the early growth phases.

Despite growth under aeration, Shewanella species had limited flux through the TCA cycle, resulting in lactate not being fully oxidized and accumulation of acetate, which is known to inhibit growth (Tang et al., 2007b). Acetate production from Shewanella MR-1 could be enhanced by oxygen uptake constraints (i.e., under low dissolved oxygen culture condition) during fast growth (Tang et al., 2007b). If the cells were to maximize their growth rate, one would expect acetyl-CoA to be fully oxidized rather than excreted as acetate, as this would produce a higher yield of ATP-equivalents per acetyl-CoA than the excretion of acetate or pyruvate. The observation that cells excreted a large fraction of the lactate as pyruvate and acetate can be explained by recent reports that metabolism is only truly geared towards biomass yield maximization under carbon scarcity in continuous cultures; rather, it has been proposed that exponentially growing cells regulate their metabolism to achieve a combination of maximizing overall ATP yield and minimizing the overall fluxes through the metabolic network (i.e., minimal enzyme usage) (Schuetz et al., 2007). Thus, ‘‘overflow’’ of acetate and pyruvate significantly reduces fluxes through central pathways and, hence, enzyme usage in the metabolic network.

Grown on lactate, the Shewanella species and E. coli had low flux through the pentose phosphate pathway which was mainly for biomass production (<3% of lactate uptake). The fluxes through the ED pathway, which allows cells to synthesize glucose-6-phosphate, were minimal. Two anapleurotic reactions appeared to be active in all Shewanella species and E. coli (malate $ pyruvate; phosphoenolpyruvate $ oxaloacetate). Fluxes through the two reactions were around 10–20% of the lactate uptake for all species. The glyoxylate shunt also had measurable flux in all species (less than 10% of the lactate uptake); this pathway reduces the amount of acetyl-CoA being com-pletely oxidized by the TCA cycle and saves carbon substrate for biosynthesis (Zhao and Shimizu, 2003).

The lack of constancy over time in key amino acid labeling profiles in all Shewanella species (using MR-1 as an example) and E. coli (Fig. 4) attests to a change in flux distribution from the early to the late phase of exponential growth, consistent with the change of the carbon sources from lactate to pyruvate and acetate. When the isotopomer data from proteinogenic amino acids in the late phase biomass were used in our isotopomer model, the calculated MR1 and E. coli flux profiles showed an increase in fluxes through the TCA cycle, specific anapleurotic reactions (PEP ! OAA), and the glyoxylate shunt (Table II). The increased flux through the TCA cycle resulted from the depletion of lactate and subsequent substitution by the previously excreted acetate as the primary carbon source. Previously, it has been shown using metabolic flux analysis that S. oneidensis MR-1 and E. coli grown under severe carbon-limited conditions had increased flux through the glyoxylate shunt or anapleurotic reactions (Fischer and Sauer, 2003; Sauer et al., 1999; Tang et al., 2007a). In the late growth phase, gluconeogenesis (necessary for biosynthesis of nucleotides and amino acids) also increased. These results indicate that there is a shift from the early phase dominated primarily by metabolite (i.e., pyruvate and acetate) excretion and energy production towards the late phase where carbon metabolism becomes more complete. Taken together, these data demonstrate the flexibility of Shewanella to alter its growth strategy and underlying metabolism in accordance with carbon source availability, that is, Shewanella spp. central metabolism tends to maximize conversion of a favorable carbon substrate (lactate) to two less energetically favorable substrates (pyruvate and acetate), which can be utilized later (E. coli only excreted acetate in the exponential growth phase). From an evolutionary view, such metabolism under unlimited growth may enable cells to compete with other organisms by quickly consuming favorable carbon sub-strates and excreting less favorable carbon sources, some of which may be inhibitory to other organisms competing in the same environment.

It must be mentioned that the amino acid labeling profiles from the late exponential phase are an average of the protein synthesized in the early exponential phase—when the cells are essentially in steady-state growth using lactate as carbon sources—and late exponential phase, where the carbon sources switch to pyruvate or acetate. Thus, the flux results based on the isotopomer data in the late exponential phase must be interpreted as the ‘‘averaged’’ flux distribution through the multiple growth stages. This is not the case for the early exponential phase fluxes, where the sole carbon substrate lactate is metabolized and a ‘‘pseudo steady’’ state can be assumed at this growth stage (Sauer et al. 1999). However, comparing the ‘‘averaged’’ fluxes from late growth phase with the fluxes from the early growth phase, we could qualitatively observe the dynamic trend of central metabo-lism during Shewanella species growth, while at the same time avoiding a dynamic fluxes analysis which is compu-tationally demanding and beyond the scope of this article.

Finally, despite different growth curves and extracellular metabolite production among the Shewanella species, the flux analysis results show very similar relative intracellular flux profiles for all the Shewanella species grown on lactate, that is, the differences in the values of most fluxes are within the measurement uncertainty (Table II). Even for E. coli, fluxes through the central metabolic pathways (not extracellular metabolites) appear to have regulation similar to the Shewanella species. Through the diversification of the Shewanella lineage, a single ancestral species evolved into multiple species that inhabit diverse environments through changes in gene content, gene function, regulation, etc. Hence, it is interesting that the metabolic flux profiles could be very similar given the evolutionary differences. This phenomenon implies that it may be useful

to understand microbial communities as assemblages of different meta-bolic types (or ‘‘metabotypes’’) in addition to phylotypes. Each metabotype would include sets of species, possibly phylogenetically different, that share a similar relative flux distribution for metabolizing the same carbon substrate. For example, when lactate is used as the carbon source, Shewanella species show a metabotype close to that of E. coli. In contrast, Shewanella species and Desulfovibrio vulgaris, another environmentally important organism, belong to completely different metabotypes for lactate metabolism (Supplementary Fig. S-3 provides a detailed comparison of metabotypes among Shewanella species, D. vulgaris (lactate as the carbon source), and E. coli) (Tang et al., 2007c; Zhao and Shimizu, 2003).

Conclusion

Our study on flux distributions in phylogenetically distant Shewanella species and E. coli reveals a remarkable similarity in the central carbon metabolism fluxes for these species. This fact prompts the introduction of the concept of a metabotype, which provides a different classification of organisms than phylotypes regarding the characterization of metabolic activity in a microbial community. Metabo-types depend on both carbon sources and phylotypes, and thus organisms with different phylotypes can have the same or similar metabotypes (e.g., Shewanella spp. vs. E. coli). The concept of a metabotype has several possible implications. First, it allows us to predict the central metabolism of close species (whose genome may not even be sequenced yet) by only studying one representative species. Second, it paves the way to model the metabolism of whole microbial ecosystems as the sum of a limited number of metabotypes instead of a myriad of phylotypes. Third, it provides a baseline for rational metabolic engineering of micro-organisms. Because a metabotype encompasses the set of fluxes that define organisms given a growth condition, one can imagine a scenario where a microbial chassis is selected on the basis of optimizing the flux leading to necessary precursor components. Furthermore, the metabotype concept may lead to quick and efficient transfer of constructs from an engineered species to another in the same metabotype that has a more suitable growth condition. On the other hand, and complementarily, we find that the Shewanella spp. display considerable flexibility in its central carbon metabolism fluxes when adapting to different carbon sources, which may be used as a competitive recourse.

We thank J. Chu for help with experiments and isotopomer analysis, N. Zamboni from ETH Zurich for useful discussion on ^{13}C based flux analysis, and P. Hugenholtz for comments and financial support of HGM. This work is part of the Virtual Institute for Microbial Stress and Survival (http://VIMSS.lbl.gov), supported by the U.S. Depart-ment of Energy, Office of Science, Office of Biological and Environ-mental Research, Genomics:GTL Program through contract DE-AC02-05CH11231 between the Lawrence Berkeley National Laboratory and the US Department of Energy, and part of the Joint BioEnergy Institute, supported by the U.S. Department of Energy.

References

Alm EJ, Huang KH, Price MN, Koche RP, Keller K, Dubchak IL, Arkin AP. 2005. The MicrobesOnline Web site for comparative genomics. Genome Res 15:1015–1022.

Antoniewicz MR, Kelleher JK, Stephanopoulos G. 2007. Accurate assess-ment of amino acid mass isotopomer distributions for metabolic flux analysis. Anal Chem 79(19):7554–7559.

Arauzo-Bravo MJ, Shimizu K. 2003. An improved method for statistical analysis of metabolic flux analysis using isotopomer mapping matrices with analytical expressions. J Biotechnol 105:117–133.

Blank LM, Kuepfer L, Sauer U. 2005. Large-scale 13C-flux analysis reveals mechanistic principles of metabolic network robustness to null muta-tions in yeast. Genome Biol 6(6):R49.

Deb K. 2001. Multi-objective optimization using evolutionary algorithms. Chichester, UK: John Wiley & Sons.

Deb K, Agarwal R. 1995 Simulated binary crossover for continuous search space. Complex Syst 9:115–148.

Deb K, Kumar A. 1995. Real-coded genetic algorithms with simulated binary crossover: Studies on multimodal and multiob jective problems. Complex Syst 9:431–454.

Fischer E, Sauer U. 2003. A novel metabolic cycle catalyzes glucose oxida-tion and anaplerosis in hungry Escherichia coli. J Biol Chem 278(47): 46446–46451.

Fischer E, Sauer U. 2005. Large-scale in vivo flux analysis shows rigidity and suboptimal performance of Bacillus subtilis metabolism. Nat Genet 37(6):636–640.

Fredrickson JK, Romine MF, Beliaev AS, Auchtung JM, Driscoll ME, Gardner TS, Nealson KH, Osterman AL, Pinchuk G, Reed JL, Rodionov DA, Rodrigues JL, Saffarini DA, Serres MH, Spormann AM, Zhulin IB, Tiedje JM. 2008. Towards environmental systems biology of Shewanella. Nat Rev Micro 6(8):592–603.

Goldberg DE. 1989. Genetic algorithms in search, optimization, and machine learning reading. Massachusetts: Addison-Wesley.

Perrenoud A, Sauer U. 2005. Impact of global transcriptional regulation by ArcA, ArcB, Cra, Crp, Cya, Fnr, and Mlc on glucose catabolism in Escherichia coli. J Bacteriol 187(9):3171–3179.

Press WH, Teukolsky SA, Vetterling WT, Flannery BP. 1992. Numerical recipes in FORTRAN. Cambridge: Cambridge University Press. pp. 387–448.

Sastry K, Goldberg DE. Modeling tournament selection with replacement using apparent added noise. 2001. pp. 129–134.

Sauer U. 2006. Metabolic networks in motion: 13C-based flux analysis. Mol Syst Biol 2:62.

Sauer U, Lasko DR, Fiaux J, Hochuli M, Glaser R, Szyperski T, Wuthrich K, Bailey JE. 1999. Metabolic flux ratio analysis of genetic and environ-mental modulations of Escherichia coli central carbon metabolism. J Bacteriol 181(21):6679–6688.

Schuetz R, Kuepfer L, Sauer U. 2007. Systematic evaluation of objective functions for predicting intracellular fluxes in Escherichia coli. Mol Syst Biol 3:119.

Tang YJ, Laidlaw D, Gani K, Keasling JD. 2006. Evaluation of the effects of various culture conditions on Cr(VI) reduction by Shewanella oneidensis MR-1 in a novel high-throughput mini-bioreactor. Biotech-nol Bioeng 95(1):176–184.

Tang YJ, Hwang JS, Wemmer D, Keasling JD. 2007a. The Shewanella oneidensis MR-1 fluxome under various oxygen conditions. Appl Environ Microbiol 73(3):718–729.

Tang YJ, Meadows AL, Keasling JD. 2007b. A kinetic model describing Shewanella oneidensis MR-1 growth, substrate consumption, and product secretion. Biotechnol Bioeng 96(1):125–133.

Tang YJ, Pingitore F, Mukhopadhyay A, Phan R, Hazen TC, Keasling JD. 2007c. Pathway confirmation and flux analysis of central metabolic pathways in Desulfovibrio vulgaris Hildenborough using GC-MS and FT-ICR mass spectrometry. J Bacteriol 189(3):940– 949.

Tiedje JM. 2002. Shewanella—The environmentally versatile genome. Nat Biotechnol 20:1093–1094.

Venkateswaran K, Moser DP, Dollhopf ME, Lies DP, Saffarini DA, Mac-Gregor BJ, Ringelberg DB, White DC, Nishijima M, Sano H, Burghardt J, Stackenbrandt E, Nealson KH. 1999. Polyphasic taxonomy of the genus Shewanella and description of Shewanella oneidensis sp. Int J Syst Bacteriol 49(Part 2):705–724.

Wahl SA, Dauner M, Wiechert W. 2004. New tools for mass isotopomer data evaluation in ^{13}C flux analysis: Mass isotope correction, data consistency checking, and precursor relationships. Biotechnol Bioeng 85(3):259–268.

Wiechert W, Mollney M, Isermann N, Wurzel M, de Graaf AA. 1999. Bidirectional reaction steps in metabolic networks: III. Explicit solution and analysis of isotopomer labeling systems. Biotechnol Bioeng 66(2): 69–85.

Zhao J, Shimizu K. 2003. Metabolic flux analysis of Escherichia coli K12 grown on 13C-labeled acetate and glucose using GC-MS and powerful flux calculation method. J Biotechnol 101:101–117.

Table I. Genetic/environmental characteristics and growth rates (in MR-1 minimal medium and 308C) for Shewanella spp.

	GC content (%)	Genome size (Mb)	Ecotype	Pathogen	Temperature	Growth rate (h^{-1})
MR1	46.0	4.97	Aquatic	X	Mesophile	0.23 ± 0.04
MR4	48.0	4.71	Marine		Mesophile	0.28 ± 0.03
MR7	49.5	4.80	Marine		Mesophile	0.29 ± 0.02
SB2B	58.0	4.31	Fresh water		Mesophile	0.24 ± 0.04
CN32	44.5	4.66	Aquatic/Soil	X	Mesophile	0.26 ± 0.05
PV4	53.8	4.60	Marine		Psychrophile	0.24 ± 0.03
ANA3	49.5	4.97	Soil		Mesophile	0.28 ± 0.06
W3-18-1	45.0	4.71	Marine/Deep Sea		Psychrophile	0.27 ± 0.06

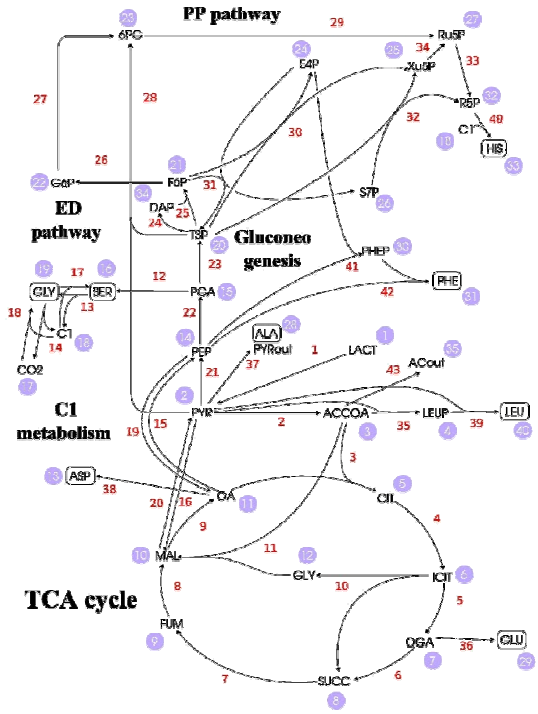

Figure 1. Central pathways of lactate metabolism in Shewanella and E. coli. The amino acids used for isotopomer models are boxed. Numbers denote the arbitrary flux indices used in modeling the pathways and circled numbers denote metabolite numbers (used for construction of reaction list in supplementary Table S-II). 6PG, 6-phosphogluconate; ACCOA, acetyl-coenzyme A; ACout, acetate outside the cell; ALA, alanine; ASP, aspartic acid; CIT, citrate; DAP, dihydroxyacetone phosphate; E4P, erythrose-4-phosphate; C1, 5,10-Me-THF; F6P, fructose-6-phosphate; FUM, fumarate; G6P, glucose-6-phosphate; GLU, glutamate; GLY (boxed), glycine; GLY, glyoxylate; HIS, histidine; ICIT, isocitrate; LACT, lactate; LEU, leucine; LEUP, leucine precursor; MAL, malate; OA, oxaloacetate; OGA, 2-oxoglutarate; PEP, phosphoenolpyruvate; PGA, 3-phosphoglycerate; PHEP, phenyalanine precursor; PHE, phenyalanine; PYR, pyruvate; R5P, ribose-5-phosphate; Ru5P, ribulose-5-phosphate; Xu5P, xylulose-5-phosphate; S7P, sedoheptulose-7-phosphate; SER, serine; SUCC, succinate; T3P, triose-3-phosphate; PYR, pyruvate. [Color figure can be seen in the online version of this article, available at www.interscience. wiley.com.]

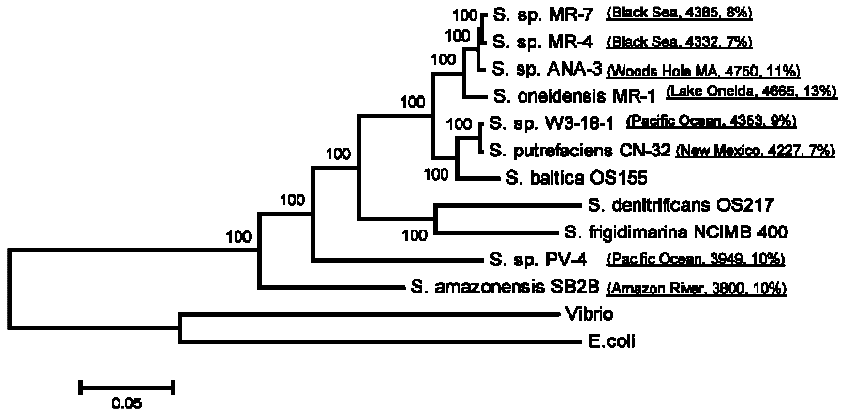

Figure 2. Phylogenetic relatedness of 11 sequenced Shewanella genomes. A maximum likelihood tree (PHYML) showing the evolutionary relationship between the Shewanella species is illustrated. The tree is based on a concatenated multiple sequence alignment of 100 single-copy genes present in all of the species. All nodes were consistent with 100 bootstraps. E. coli and Vibrio cholerae were used as the outgroups. Eight Shewanella species were studied, and the parenthesis includes the source of species, number of genes, and percent of unique genes not found by sequence homology in the other ten Shewanella genomes. The detailed information about all Shewanella strains can be found at the Shewanella federation website: www.shewanella.org.

Figure 3. Growth kinetics of Shewanella oneidensis MR-1 and other species. a: Shewanella and E. coli growth kinetics (&) MR-4, (~) MR-7, (*) ANA-3, (^) PV-4, (^) SB2B, (&) W3-18-1, (*) CN-32, (~:) MR-1, (3) E. coli W3110. b: Substrate consumption and product excretion kinetics in Shewanella species (using MR-1 as an example) and W3110. (&) lactate (MR-1), (^) acetate (MR-1), (*) pyruvate (MR-1), (&) lactate (E. coli W3110), (^) acetate (E. coli W3110).

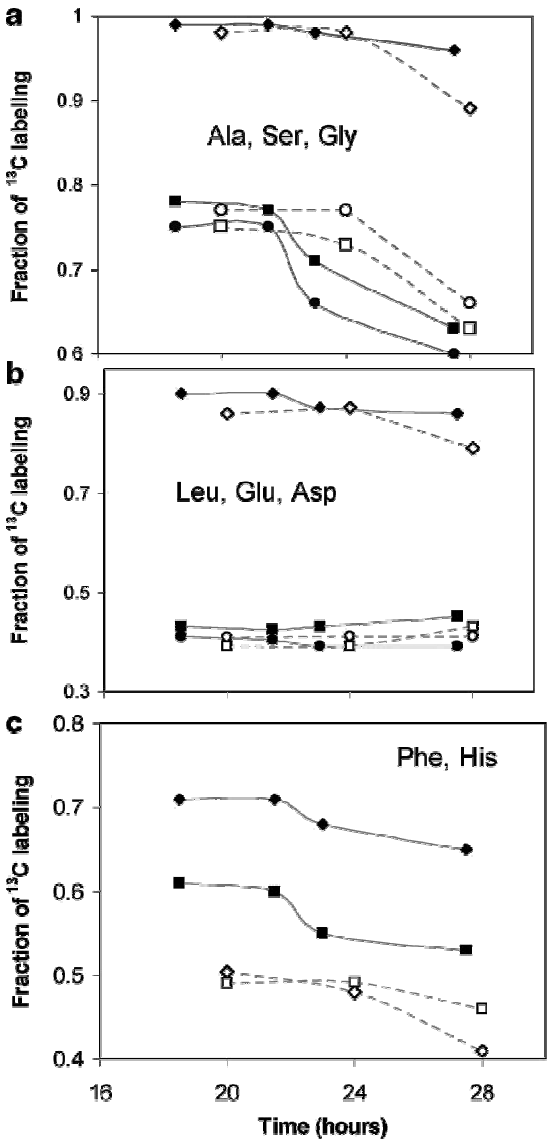

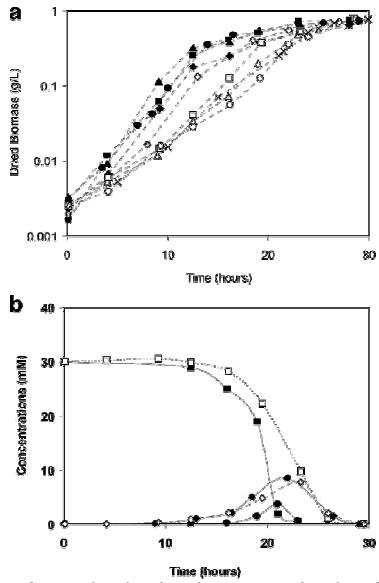

Figure 4. Labeling fraction of most abundant ion changes as a function of time showing the isotopomer shifting in proteinogenic amino acids during MR-1 and E. coli W3110 growth. M0, M1, M2. . . represent unlabeled, singly ^{13}C labeled, and doubly ^{13}C labeled mass ions, respectively, of a given amino acid. The constancy over time in key amino acid labeling profiles in all Shewanella species (using MR-1 as an example) and E. coli shows that an isotopomer steady state is reached in the early growth stage. A marked change in these same profiles indicates a shift in flux at later stages. a: Amino acids (precursors from gluconeogenesis and serine metabolism pathway) (&) Ser (M1 [-57], MR-1), (*) Gly (M1 [-57], MR-1), (^) Ala (M1 [-57], MR-1), (&) Ser (M1 [-57], E. coli), (*) Gly (M1 [-57], E. coli), ^: Ala (M1 [-57], E. coli). b: Amino acids (precursors from TCA cycle) (&) Glu (M3 [-57], MR-1), (*) Asp (M2 [-57], MR-1), (^) Leu (M3 [-159], MR-1), (&) Glu (M3 [-57], E. coli), (*) Asp (M2 [-57], E. coli), (^) Leu (M3 [-159], E. coli). c: Amino acids (precursors from gluconeogenesis and pentose phosphate pathway). (&) His (M1 [-57], MR-1), (^) Phe (M1 [-57], MR-1), (&) His (M1 [-57], E. coli), (^) Phe (M1 [-57], E. coli).

Table II. Comparison of central carbon metabolism (flux/confidence interval) among the different Shewanella species and E. coli W3110.

Flux no.	MR1	MR4	MR7	SB	CN	W3	ANA	PV4	E. coli	MR1 late	E. coli late
TCA cycle þ lactate uptake (TCA)											
1	1.00/0.00	1.00/0.00	1.00/0.00	1.00/0.00	1.00/0.00	1.00/0.00	1.00/0.00	1.00/0.00	1.00/0.00	1.00/0.00	1.00/0.00
2	0.72/0.15	0.90/0.15	0.90/0.12	0.82/0.18	0.74/0.12	0.86/0.15	0.83/0.14	0.89/0.13	0.94/0.16	0.86/0.18	1.07/0.23
3	0.36/0.13	0.34/0.11	0.30/0.09	0.53/0.18	0.42/0.14	0.43/0.15	0.39/0.12	0.32/0.09	0.39/0.14	0.76/0.18	0.75/0.19
4	0.36/0.13	0.34/0.11	0.30/0.09	0.53/0.18	0.42/0.14	0.43/0.15	0.39/0.12	0.32/0.09	0.39/0.14	0.76/0.18	0.75/0.19
5	0.30/0.10	0.24/0.07	0.20/0.08	0.46/0.16	0.39/0.13	0.38/0.12	0.32/0.09	0.21/0.06	0.32/0.09	0.66/0.15	0.57/0.13
6	0.28/0.09	0.23/0.07	0.19/0.08	0.45/0.17	0.38/0.13	0.36/0.13	0.31/0.10	0.20/0.06	0.30/0.09	0.65/0.16	0.56/0.13
7	0.34/0.13	0.32/0.11	0.29/0.10	0.52/0.19	0.40/0.13	0.42/0.15	0.38/0.13	0.31/0.10	0.37/0.14	0.75/0.19	0.74/0.19
8	0.34/0.13	0.32/0.11	0.29/0.10	0.52/0.19	0.40/0.13	0.42/0.15	0.38/0.13	0.31/0.10	0.37/0.14	0.75/0.19	0.74/0.19
9	0.29/0.08	0.25/0.07	0.18/0.04	0.38/0.11	0.33/0.08	0.31/0.08	0.28/0.06	0.22/0.05	0.30/0.08	0.65/0.13	0.63/0.13
Glyoxylate shunt (GSH)											
10	0.06/0.04	0.10/0.07	0.10/0.06	0.07/0.04	0.03/0.02	0.05/0.03	0.07/0.05	0.11/0.06	0.07/0.05	0.10/0.04	0.17/0.09
11	0.06/0.04	0.10/0.07	0.10/0.06	0.07/0.04	0.03/0.02	0.05/0.03	0.07/0.05	0.11/0.06	0.07/0.05	0.10/0.04	0.17/0.09
Reversible net fluxes and C1 metabolism (RN)											
12	0.02/0.03	0.01/0.03	0.01/0.03	0.02/0.02	0.02/0.03	0.02/0.03	0.02/0.03	0.02/0.02	0.02/0.03	0.03/0.02	0.02/0.03
13	0.03/0.07	0.01/0.05	0.01/0.06	0.06/0.07	0.02/0.09	0.02/0.04	0.03/0.05	0.03/0.08	0.04/0.09	0.10/0.11	0.11/0.69
14	0.03/0.05	0.01/0.06	0.01/0.07	0.03/0.04	0.02/0.05	0.03/0.05	0.02/0.04	0.02/0.03	0.02/0.03	0.05/0.05	0.02/0.06
15	0.00/0.02	0.00/0.01	0.00/0.04	0.00/0.03	0.00/0.01	0.00/0.01	0.00/0.01	0.00/0.02	0.03/0.02	0.00/0.00	0.03/0.05
16	0.00/0.03	0.00/0.04	0.00/0.04	0.00/0.02	0.00/0.03	0.00/0.04	0.00/0.04	0.00/0.04	0.00/0.04	0.00/0.03	0.00/0.04
Reversible exchange (RE)											
17	0.01/0.05	0.00/0.03	0.00/0.04	0.04/0.06	0.00/0.08	0.00/0.01	0.01/0.03	0.01/0.06	0.02/0.08	0.07/0.09	0.09/0.69
18	0.01/0.02	0.00/0.04	0.00/0.05	0.01/0.02	0.01/0.01	0.01/0.02	0.01/0.01	0.00/0.01	0.00/0.01	0.02/0.03	0.01/0.04
19	0.08/0.04	0.10/0.06	0.14/0.07	0.16/0.07	0.11/0.05	0.13/0.06	0.12/0.05	0.11/0.05	0.13/0.07	0.12/0.04	0.17/0.09
20	0.11/0.08	0.17/0.11	0.22/0.10	0.20/0.10	0.10/0.05	0.16/0.08	0.17/0.09	0.20/0.09	0.14/0.08	0.20/0.08	0.28/0.12
Glycolysis (Gly)											
21	0.16/0.04	0.17/0.04	0.19/0.04	0.22/0.04	0.19/0.04	0.21/0.04	0.21/0.03	0.19/0.04	0.16/0.03	0.25/0.05	0.18/0.07
22	0.05/0.06	0.05/0.05	0.03/0.04	0.04/0.05	0.06/0.06	0.05/0.06	0.06/0.04	0.06/0.03	0.04/0.05	0.11/0.05	0.03/0.07
23	0.03/0.04	0.04/0.03	0.02/0.02	0.02/0.04	0.04/0.04	0.03/0.04	0.05/0.03	0.04/0.02	0.02/0.03	0.07/0.04	0.01/0.05
24	0.01/0.01	0.02/0.01	0.01/0.01	0.00/0.01	0.02/0.01	0.01/0.01	0.02/0.01	0.01/0.01	0.01/0.01	0.03/0.01	0.00/0.02
25	0.01/0.01	0.02/0.01	0.01/0.01	0.00/0.01	0.02/0.01	0.01/0.01	0.02/0.01	0.01/0.01	0.01/0.01	0.03/0.01	0.00/0.02
26	0.01/0.01	0.02/0.01	0.01/0.01	0.00/0.01	0.02/0.01	0.01/0.01	0.02/0.01	0.01/0.01	0.01/0.00	0.03/0.02	0.00/0.01
Pentose phosphate þ ED pathway (PPP)											
27	0.01/0.01	0.02/0.01	0.01/0.01	0.00/0.01	0.02/0.01	0.01/0.01	0.02/0.01	0.01/0.01	0.01/0.00	0.03/0.02	0.00/0.01
28	0.00/0.01	0.00/0.01	0.00/0.01	0.01/0.02	0.00/0.01	0.00/0.01	0.01/0.01	0.01/0.01	0.00/0.01	0.00/0.01	0.00/0.01
29	0.02/0.02	0.02/0.01	0.01/0.01	0.01/0.02	0.02/0.02	0.01/0.02	0.02/0.02	0.02/0.01	0.01/0.01	0.04/0.02	0.01/0.02
30	0.01/0.01	0.01/0.01	0.01/0.01	0.01/0.01	0.01/0.01	0.01/0.01	0.01/0.01	0.01/0.01	0.01/0.01	0.01/0.02	0.01/0.01
31	0.01/0.00	0.01/0.00	0.01/0.00	0.01/0.01	0.01/0.00	0.01/0.00	0.01/0.00	0.01/0.00	0.01/0.00	0.01/0.01	0.01/0.01
32	0.01/0.00	0.01/0.00	0.01/0.00	0.01/0.01	0.01/0.00	0.01/0.00	0.01/0.00	0.01/0.00	0.01/0.00	0.01/0.01	0.01/0.01
33	0.02/0.02	0.02/0.01	0.01/0.01	0.01/0.02	0.02/0.02	0.01/0.02	0.02/0.02	0.02/0.01	0.01/0.02	0.04/0.02	0.01/0.03
34	0.00/0.01	0.00/0.01	0.00/0.01	0.00/0.01	0.00/0.01	0.00/0.01	0.00/0.01	0.00/0.01	0.00/0.01	0.00/0.01	0.00/0.01
Amino acids and external (AM þ ext)											
35	0.01/0.01	0.01/0.01	0.01/0.01	0.01/0.01	0.01/0.01	0.01/0.01	0.01/0.01	0.01/0.01	0.01/0.01	0.01/0.02	0.01/0.01
36	0.02/0.01	0.01/0.00	0.01/0.00	0.01/0.01	0.02/0.01	0.01/0.01	0.01/0.01	0.01/0.01	0.01/0.01	0.01/0.01	0.01/0.00
37	0.20/0.03	0.08/0.03	0.11/0.02	0.13/0.03	0.14/0.02	0.06/0.03	0.11/0.02	0.08/0.02	0.02/0.02	0.06/0.03	0.01/0.03
38	0.01/0.02	0.01/0.02	0.01/0.01	0.01/0.02	0.01/0.02	0.01/0.01	0.01/0.02	0.01/0.02	0.01/0.01	0.01/0.02	0.01/0.02
39	0.01/0.01	0.01/0.01	0.01/0.01	0.01/0.01	0.01/0.01	0.01/0.01	0.01/0.01	0.01/0.01	0.01/0.01	0.01/0.02	0.01/0.01
40	0.01/0.02	0.01/0.02	0.00/0.01	0.00/0.02	0.01/0.02	0.01/0.02	0.02/0.02	0.01/0.01	0.00/0.01	0.03/0.02	0.00/0.02
41	0.01/0.01	0.01/0.01	0.01/0.01	0.01/0.02	0.01/0.01	0.01/0.01	0.01/0.01	0.01/0.01	0.01/0.01	0.01/0.02	0.01/0.02
42	0.01/0.01	0.01/0.01	0.01/0.01	0.01/0.02	0.01/0.01	0.01/0.01	0.01/0.01	0.01/0.01	0.01/0.01	0.01/0.02	0.01/0.02
43	0.29/0.02	0.46/0.03	0.48/0.02	0.21/0.03	0.29/0.03	0.37/0.03	0.35/0.03	0.45/0.02	0.47/0.02	0.01/0.03	0.14/0.03